

1 **A GENERALISED RANDOM ENCOUNTER MODEL FOR ESTIMATING**
2 **ANIMAL DENSITY WITH REMOTE SENSOR DATA**

3 **Running title: A generalised random encounter model for animals.**

4 **Word count:**

5 **Authors:**

6 Tim C.D. Lucas^{1,2,3}, Elizabeth A. Moorcroft^{1,4,5}, Robin Freeman⁵, Marcus J. Rowcliffe⁵,
7 Kate E. Jones^{2,5}

8 **Addresses:**

9 1 CoMPLEX, University College London, Physics Building, Gower Street, Lon-
10 don, WC1E 6BT, UK

11 2 Centre for Biodiversity and Environment Research, Department of Genetics,
12 Evolution and Environment, University College London, Gower Street, London,
13 WC1E 6BT, UK

14 3 Department of Statistical Science, University College London, Gower Street,
15 London, WC1E 6BT, UK

16 4 Department of Computer Science, University College London, Gower Street,
17 London, WC1E 6BT, UK

18 5 Institute of Zoology, Zoological Society of London, Regents Park, London, NW1
19 4RY, UK

20 **Corresponding authors:**

21 Kate E. Jones,
22 Centre for Biodiversity and Environment Research,
23 Department of Genetics, Evolution and Environment,
24 University College London,
25 Gower Street,
26 London,
27 WC1E 6BT,
28 UK

29 kate.e.jones@ucl.ac.uk

30

31 Marcus J. Rowcliffe,

32 Institute of Zoology,

33 Zoological Society of London,

34 Regents Park,

35 London,

36 NW1 4RY,

37 UK

38 marcus.rowcliffe@ioz.ac.uk

ABSTRACT

39
40 **1:** Wildlife monitoring technology has advanced rapidly and the use of remote
41 sensors such as camera traps, and acoustic detectors is becoming common in both
42 the terrestrial and marine environments. Current methods to estimate abundance
43 or density require individual recognition of animals or knowing the distance of
44 the animal from the sensor, which is often difficult. A method without these re-
45 quirements, the random encounter model (REM), has been successfully applied to
46 estimate animal densities from count data generated from camera traps. However,
47 count data from acoustic detectors do not fit the assumptions of the REM due to
48 the directionality of animal signals.

49 **2:** We developed a generalised REM (gREM), to estimate absolute animal density
50 from count data from both camera traps and acoustic detectors. We derived the
51 gREM for different combinations of sensor detection widths and animal signal
52 widths (a measure of directionality). We tested the accuracy and precision of this
53 model using simulations of different combinations of sensor detection widths and
54 animal signal widths, number of captures, and models of animal movement.

55 **3:** We find that the gREM produces accurate estimates of absolute animal density
56 for all combinations of sensor detection widths and animal signal widths. How-
57 ever, larger sensor detection and animal signal widths were found to be more pre-
58 cise. While the model is accurate for all capture efforts tested, the precision of the
59 estimate increases with the number of captures. We found no effect of different
60 animal movement models tested on the accuracy and precision of the gREM.

61 **4:** We conclude that the gREM provides an effective method to estimate absolute
62 animal densities from remote sensor count data over a range of sensor and animal
63 signal widths. The gREM is applicable for count data obtained in both marine and
64 terrestrial environments, visually or acoustically (e.g., big cats, sharks, birds, bats
65 and cetaceans). As sensors such as camera traps and acoustic detectors become
66 more ubiquitous, the gREM will be increasingly useful for monitoring unmarked
67 animal populations across broad spatial, temporal and taxonomic scales.

Keywords. acoustic detection, camera traps, marine, population monitoring, simulations, terrestrial

INTRODUCTION

Animal population density is one of the fundamental measures needed in ecology and conservation. The density of a population has important implications for a range of issues such as sensitivity to stochastic fluctuations (Richter-Dyn & Goel, 1972; Wright & Hubbell, 1983) and risk of extinction (Purvis *et al.*, 2000). Monitoring animal population changes in response to anthropogenic pressure is becoming increasingly important as humans modify habitats and change climates as never before (Everatt *et al.*, 2014). Sensor technology, such as camera traps (Karanth, 1995; Rowcliffe & Carbone, 2008) and acoustic detectors (Clark, 1995; O’Farrell & Gannon, 1999; Acevedo & Villanueva-Rivera, 2006) are becoming increasingly used to monitor changes in animal populations (Rowcliffe & Carbone, 2008; Kessel *et al.*, 2014), as they are efficient, relatively cheap and non-invasive (Cutler & Swann, 1999), allowing for surveys over large areas and long periods. However, the problem of converting sampled count data to estimates of density remains as efforts must be made to account for detectability of the animals (Anderson, 2001).

Methods do already exist for estimating animal density but these methods often require additional information that may not be available. For example, capture-mark-recapture methods (Karanth, 1995; Trolle & Kéry, 2003; Soisalo & Cavalcanti, 2006; Trolle *et al.*, 2007; Borchers *et al.*, 2014) require recognition of individuals, distance methods (Harris *et al.*, 2013) require an estimation of how far away individuals are from the sensor (Barlow & Taylor, 2005; Marques *et al.*, 2011). The development of the random encounter model (REM) (a modification of a gas model) enabled animal densities to be estimated from unmarked individuals of a known speed, and sensor detection parameters (Rowcliffe *et al.*, 2008). The REM method has been successfully applied to estimate animal densities from camera trap surveys (Manzo *et al.*, 2012; Zero *et al.*, 2013). However, extending the REM method to other types of sensors (for example acoustic detectors) is more problematic, because the original derivation assumes a relatively narrow sensor width (up to $\pi/2$

99 radians) and that the animal is equally detectable irrespective of its heading (Row-
100 cliffe *et al.*, 2008).

101 Whilst these restrictions are not problematic for most camera trap makes (e.g.
102 Reconyx, Cuddeback), the REM could not be used to estimate densities from cam-
103 era traps with a wider sensor width (e.g. canopy monitoring with fish eye lens
104 (Brusa & Bunker, 2014)). Additionally, the REM method would not be useful in
105 estimating densities from acoustic survey data as the acoustic detector angles are
106 often wider than $\pi/2$ radians. Acoustic detectors are designed for a range of di-
107 verse tasks and environments (Kessel *et al.*, 2014), which will naturally lead to a
108 wide range of sensor detection widths and detection distances. In addition to this,
109 calls emitted by many animals are directional (Blumstein *et al.*, 2011) breaking the
110 assumption of the REM method.

111 There has been a sharp rise in interest around passive acoustic detectors in re-
112 cent years, with a 10 fold increase in publications in the decade between 2000 and
113 2010 (Kessel *et al.*, 2014). Acoustic monitoring is being developed to study many
114 aspects of ecology, including the interactions of animals and their environments
115 (Blumstein *et al.*, 2011; Rogers *et al.*, 2013), the presence and relative abundances of
116 species (Marcoux *et al.*, 2011), and biodiversity of an area (Depraetere *et al.*, 2012).

117 Acoustic data suffers from many of the problems associated with data from
118 camera trap surveys in that individuals are often unmarked so capture-mark-
119 recapture methods cannot be used to estimate densities. In some cases the dis-
120 tance between the animal and the sensor is known, for example when an array of
121 sensors and the position of the animal is estimated by triangulation (Lewis *et al.*,
122 2007). In these situations distance-sampling methods can be applied, a method
123 typically used for marine mammals (Rogers *et al.*, 2013). However, in many cases
124 distance estimation is not possible, for example when single sensors are deployed,
125 a situation typical in the majority of terrestrial acoustic surveys (Elphick, 2008;
126 Buckland *et al.*, 2008). In these cases, only relative measures of local abundance can
127 be calculated, and not absolute densities. This means that comparison of popula-
128 tions between species and sites is problematic without assuming equal detectabil-
129 ity (Hayes, 2000; Schmidt, 2003; Adams *et al.*, 2013). Equal detectability is unlikely

130 because of differences in environmental conditions, sensor type, habitat, species
131 biology.

132 In this study we create a generalised REM (gREM), as an extension to the cam-
133 era trap model of (Rowcliffe *et al.*, 2008), to estimate absolute density from count
134 data from acoustic detectors, or camera traps, where the sensor width can vary
135 from 0 to 2π radians, and the signal given from the animal can be directional. We
136 assessed the accuracy and precision of the gREM within a simulated environment,
137 by varying the sensor detection widths, animal signal widths, number of captures
138 and models of animal movement. We use the simulation results to recommend
139 best survey practice for estimating animal densities from remote sensors.

140 METHODS

141 **Analytical Model.** The REM presented by Rowcliffe *et al.* (2008) adapts the gas
142 model to model count data from camera trap surveys. The REM is derived assum-
143 ing a stationary sensor with a detection width less than $\pi/2$ radians. However, in
144 order to apply this approach more generally, and in particular to acoustic detec-
145 tors, we need both to relax the constraint on sensor detection width, and allow
146 for animals with directional signals. Consequently, we derive the gREM for any
147 detection width, θ , between 0 and 2π with a detection distance r giving a circular
148 sector within which animals can be captured (the detection zone)(Figure 1). Ad-
149 ditionally, we model the animal as having an associated signal width α between
150 0 and 2π (Figure 1, see Appendix S1 for a list of symbols). We start deriving the
151 gREM with the simplest situation, the gas model where $\theta = 2\pi$ and $\alpha = 2\pi$.

152 *Gas Model.* Following Yapp (1956), we derive the gas model where sensors can
153 capture animals in any direction and animal's signal is detectable from any direc-
154 tion ($\theta = 2\pi$ and $\alpha = 2\pi$). We assume that animals are in a homogeneous environ-
155 ment, and move in straight lines of random direction with velocity v . We allow
156 that our stationary sensor can capture animals at a detection distance r and that if
157 an animal moves within this detection zone they are captured with a probability
158 of one, while animals outside the zone are never captured.

159 In order to derive animal density, we need to consider relative velocity from
160 the reference frame of the animals. Conceptually, this requires us to imagine that

all animals are stationary and randomly distributed in space, while the sensor moves with velocity v . If we calculate the area covered by the sensor during the survey period we can estimate the number of animals the sensor should capture. As a circle moving across a plane, the area covered by the sensor per unit time is $2rv$. The number of expected captures, z , for a survey period of t , with an animal density of D is $z = 2rvtD$. To estimate the density, we rearrange to get $D = z/2rvt$.

gREM derivations for different detection and signal widths. Different combinations of θ and α would be expected to occur (e.g., sensors have different detection widths and animals have different signal widths). For different combinations θ and α , the area covered per unit time is no longer given by $2rv$. Instead of the size of the sensor detection zone having a diameter of $2r$, the size changes with the approach angle between the sensor and the animal. For any given signal width and detector width and depending on the angle that the animal approaches the sensor, the width of the area within which an animal can be detected is called the profile, p . The size of the profile (averaged across all approach angles) is defined as the average profile \bar{p} . However, different combinations of θ and α need different equations to calculate \bar{p} .

We have identified the parameter space for the combinations of θ and α for which the derivation of the equations are the same (defined as sub-models in the gREM) (Figure 2). For example, the gas model becomes the simplest gREM sub-model (upper right in Figure 2) and the REM from Rowcliffe *et al.* (2008) is another gREM sub-model where $\theta < \pi/2$ and $\alpha = 2\pi$. We derive one gREM sub-model SE2 as an example below, where $2\pi - \alpha/2 < \theta < 2\pi$, $0 < \alpha < \pi$ (see Appendix S2 for other gREM sub-models).

Example derivation of SE2. In order to calculate \bar{p} , we have to integrate over the focal angle, x_1 (Figure 3a). This is the angle taken from the centre line of the sensor. Other focal angles are possible (x_2, x_3, x_4) and are used in other gREM sub-models (see Appendix S2). As the size of the profile depends on the approach angle, we present the derivation across all approach angles. When the sensor is directly approaching the animal $x_1 = \pi/2$.

191 Starting from $x_1 = \pi/2$ until $\theta/2 + \pi/2 - \alpha/2$, the size of the profile is $2r \sin \alpha/2$
 192 (Figure 3b). During this first interval, the size of α limits the width of the profile.
 193 When the animal reaches $x_1 = \theta/2 + \pi/2 - \alpha/2$ (Figure 3c), the size of the profile is
 194 $r \sin(\alpha/2) + r \cos(x_1 - \theta/2)$ and the size of θ and α both limit the width of the profile
 195 (Figure 3c). Finally, at $x_1 = 5\pi/2 - \theta/2 - \alpha/2$ until $x_1 = 3\pi/2$, the width of the profile
 196 is again $2r \sin \alpha/2$ (Figure 3d) and the size of α again limits the width of the profile.
 197 The profile width p for π radians of rotation (from directly towards the sensor
 198 to directly behind the sensor) is completely characterised by the three intervals
 199 (Figure 3b–d). Average profile width \bar{p} is calculated by integrating these profiles
 200 over their appropriate intervals of x_1 and dividing by π which gives

$$\bar{p} = \frac{1}{\pi} \left(\int_{\frac{\pi}{2}}^{\frac{\pi}{2} + \frac{\theta}{2} - \frac{\alpha}{2}} 2r \sin \frac{\alpha}{2} dx_1 + \int_{\frac{\pi}{2} + \frac{\theta}{2} - \frac{\alpha}{2}}^{\frac{5\pi}{2} - \frac{\theta}{2} - \frac{\alpha}{2}} r \sin \frac{\alpha}{2} + r \cos \left(x_1 - \frac{\theta}{2} \right) dx_1 + \int_{\frac{5\pi}{2} - \frac{\theta}{2} - \frac{\alpha}{2}}^{\frac{3\pi}{2}} 2r \sin \frac{\alpha}{2} dx_1 \right) \quad \text{eqn 1}$$

$$= \frac{r}{\pi} \left(\theta \sin \frac{\alpha}{2} - \cos \frac{\alpha}{2} + \cos \left(\frac{\alpha}{2} + \theta \right) \right) \quad \text{eqn 2}$$

201 We then use this expression to calculate density

$$202 \quad D = z/vt\bar{p}. \quad \text{eqn 3}$$

203 Rather than having one equation that describes \bar{p} globally, the gREM must be
 204 split into submodels due to discontinuous changes in p as α and β change. These
 205 discontinuities can occur for a number of reasons such as a profile switching be-
 206 tween being limited by α and θ , the difference between very small profiles and
 207 profiles of size zero and the fact that the width of a sector stops increasing once
 208 the central angle reaches π radians (i.e., a semi circle is just as wide as a full circle.)

209 As a visual example, if α is small, there is an interval between Figure 3c and 3d
 210 where the ‘blind spot’ would prevent animals being detected at all giving $p = 0$.
 211 This would require an extra integral in our equation as simply putting our small
 212 value of α into eqn 1 would not give us this integral of $p = 0$.

213 gREM submodel specifications were done by hand, and the integration was
 214 done using SymPy (SymPy Development Team, 2014) in Python (Appendix S3).

215 The gREM submodels were checked by confirming that: (1) submodels adjacent
 216 in parameter space were equal at the boundary between them; (2) submodels that
 217 border $\alpha = 0$ had $p = 0$ when $\alpha = 0$; (3) average profile widths \bar{p} were between 0
 218 and $2r$ and; (4) each integral, divided by the range of angles that it was integrated
 219 over, was between 0 and $2r$. The scripts for these tests are included in Appendix
 220 S3 and the R (Team, 2014) implementation of the gREM is given in Appendix S4.

221 **Simulation Model.** We tested the accuracy and precision of the gREM by devel-
 222 oping a spatially explicit simulation of the interaction of sensors and animals using
 223 different combinations of sensor detection widths, animal signal widths, number
 224 of captures, and models of animal movement. 100 simulations were run where
 225 each consisted of a 7.5 km by 7.5 km square with periodic boundaries. A station-
 226 ary sensor of radius r was set up in the exact centre of each simulation, covering
 227 seven sensor detection widths θ between 0 and 2π ($2/9\pi, 4/9\pi, 6/9\pi, 8/9\pi, 10/9\pi,$
 228 $14/9\pi, 2\pi$). Each simulation was populated with a density of 70 animals km^{-2} , cal-
 229 culated from the equation in Damuth (1981) as the expected density of mammals
 230 of weighing 1 g. This density therefore represents a reasonable estimate of density
 231 of individuals, given that the smallest mammal is around 2 g (Jones *et al.*, 2009).
 232 A total of 3937 individuals per simulation were created which were placed ran-
 233 domly at the start of the simulation. Individuals were assigned 11 signal widths
 234 α between 0 and π ($1/11\pi, 2/11\pi, 3/11\pi, 4/11\pi, 5/11\pi, 6/11\pi, 7/11\pi, 8/11\pi, 9/11\pi,$
 235 $10/11\pi, \pi$).

236 Each simulation lasted for N steps (14400) of duration T (15 minutes) giving a
 237 total duration of 150 days. The individuals moved within each step with a dis-
 238 tance d , with an average speed, v . d , was sampled from a normal distribution
 239 with mean distance, $\mu_d = vT$, and standard deviation $\sigma_d = vT/10$. An average
 240 speed, $v = 40 \text{ km day}^{-1}$, was chosen as this is the largest day range of terrestrial an-
 241 imals (Carbone *et al.*, 2005), and represents the upper limit of realistic speeds. At
 242 the end step, individuals were allowed to either remain stationary for a time step
 243 (with a given probability, S), or change direction (in a uniform distribution with a
 244 maximum angle, A) between 0 and π . This resulted in seven different movement
 245 models where: (1) simple movement, where S and $A = 0$; (2) stop-start movement,

246 where (i) $S = 0.25$, $A = 0$, (ii) $S = 0.5$, $A = 0$, (iii) $S = 0.75$, $A = 0$; (3) random walk
 247 movement, where (i) $S = 0$, $A = \pi/3$, (ii) $S = 0$, $A = 2\pi/3$, (iii) $S = 0$, $A = \pi$. Individuals
 248 were counted as they moved in and out of the detection zone of the sensor per
 249 simulation.

250 We calculated the estimated animal density from the gREM by summing the
 251 number of captures per simulation and inputting these values into the correct
 252 gREM submodel. gREM accuracy was determined by comparing the density in
 253 the simulation with the estimated density. High accuracy is indicated by the mean
 254 difference between the estimated and actual values not being significantly differ-
 255 ent from zero (Wilcoxon signed-rank test). gREM precision was determined by
 256 the standard deviation of estimated densities. We used this method to compare
 257 the accuracy and precision of all the gREM submodels. As these submodels are
 258 derived for different combinations of α and θ , the accuracy and precision of the
 259 submodels was used to determine the impact of different values of α and θ .

260 The influence of the number of captures and animal movement models on ac-
 261 curacy and precision was investigated using four different gREM submodels rep-
 262 resentative of the range α and θ values (submodels NW1, SW1, NE1, and SE3, Fig-
 263 ure 2). Using these four submodels, we calculated how long the simulation needed
 264 to run to generate a range of different capture numbers (from 10 to 100 captures in
 265 10 unit intervals), and estimated animal density. These estimated densities were
 266 compared to the real density to assess the impact on the accuracy and precision of
 267 the gREM. The gREM assumes that individuals move continuously with straight-
 268 line movement (simple movement model) and we therefore assessed the impact
 269 of breaking the gREM assumptions. We used the four submodels to compare the
 270 accuracy and precision of a simple movement model, stop-start movement models
 271 and random walk movement models.

RESULTS

Analytical model. The equation for \bar{p} has been newly derived for each submodel in the gREM, except for the gas model and REM which have been calculated previously. However, many models, although derived separately, have the same expression for \bar{p} . Figure 4 shows the expression for \bar{p} in each case. The general equation for density, using the correct expression for \bar{p} is then substituted into eqn 3. Although more thorough checks are performed in Appendix S3, it can be seen that all adjacent expressions in Figure 4 are equal when expressions for the boundaries between them are substituted in.

Simulation model.

gREM submodels. All gREM submodels showed a high accuracy, i.e., the mean difference between the estimated and actual values was not significantly different from zero across all models, corrected for multiple tests (all gREM sub models Wilcoxon signed-rank test, $p > 0.002$)(Figure 5). However, the precision of the submodels do vary, where the gas model is the most precise and the SW7 sub model the least precise, having the smallest and the largest interquartile range, respectively (Figure 5). The standard deviation of the error between the estimated and true densities is strongly related to both the sensor and signal widths (Figure 6), such that larger widths have lower standard deviations (greater precision).

Number of captures. Within the four gREM submodels tested (NW1, SW1, SE3, NE1), the accuracy was not affected by the number of captures, where the mean difference between the estimated and actual values was not significantly different from zero across all capture rates, corrected for multiple tests (all gREM sub models Wilcoxon signed-rank test, $p > 0.008$)(Figure 7). However, the precision was dependent on the number of captures across all four of the gREM submodels, where precision increases as number of captures increases (Figure 7). For all gREM submodels, the the coefficient of variation falls to 10% at 100 captures.

Movement models. Within the four gREM submodels tested (NW1, SW1, SE3, NE1), neither the accuracy or precision was affected by the amount of time spent stationary. The mean difference between the estimated and actual values was not

significantly different from zero for each category of stationary time (0, 0.25, 0.5 and 0.75), corrected for multiple tests (all gREM sub models Wilcoxon signed-rank test, $p > 0.12$)(Figure 8a). Altering the maximum change in direction in each step (0, $\pi/3$, $2\pi/3$, and π) did not affect the accuracy or precision of the four gREM submodels tested (all gREM sub models Wilcoxon signed-rank test, $p > 0.05$)(Figure 8b).

DISCUSSION

We have developed the gREM such that it can be used to estimate density from acoustic sensors and camera traps. This has entailed a generalisation of the model and the REM in Rowcliffe *et al.* (2008) to be applicable to any combination of sensor width and signal directionality. We have used simulations to show, as a proof of principle, that these models are accurate and precise. The precision of the gREM was found to be dependent on the width of the sensor and the call, and the number of captures.

Analytical model. The gREM was derived for different combinations of α and θ resulting in 25 different submodels, the expression for \bar{p} are equal for many of these submodels resulting in eight different equations including the previously derived gas model and REM. These submodels were tested for consistency with adjacent expressions being equal at their boundaries. These new submodels will allow researchers to evaluate the absolute density of animals that have previously been difficult to study, such as bats (Clement & Castleberry, 2013), with noninvasive methods such as remote sensors. The gREM allows the data from acoustic detectors to be used where an animal has a directional calls, this could be used for a range of animals including songbirds (Blumstein *et al.*, 2011), and dolphins (Lammers & Au, 2003).

There are a number of possible extensions to the gREM which could be developed in the future. The original gas model was formulated for the case where both subjects, either animal and detector, or animal and animal, are moving (Hutchinson & Waser, 2007). Indeed any of the models with animals that are equally detectable in all directions ($\alpha = 2\pi$) can be trivially expanded for moving by substituting the sum of the average animal velocity and the sensor velocity for v as used

here. However, when the animal has a directional call, as seen in both terrestrial and aquatic environments (Lammers & Au, 2003; Blumstein *et al.*, 2011), the extension becomes less simple. The approach would be to calculate again the mean profile width. However, for each angle of approach, one would have to average the profile width for an animal facing in any direction (i.e. not necessarily moving towards the sensor) weighted by the relative velocity of that direction. There are a number of situations where a moving detector and animal could occur, e.g. an acoustic detector towed from a boat when studying porpoises (Kimura *et al.*, 2014) or surveying bats from a moving car (Ahlen & Baagøe, 1999; Jones *et al.*, 2013).

An interesting but unstudied problem is edge effects caused by trigger delays (the delay between sensing an animal and attempting to record the encounter) (Rovero *et al.*, 2013) and time expansion acoustic detectors which repeatedly turn on an off during sampling (Ahlen & Baagøe, 1999). Both of these have potential biases as animals can move through the detection zone without being detected. The models herein are formulated assuming constant surveillance and so the error created by switching the sensor on and off quickly becomes negligible if the sensor is on for extended periods of time. For example, if it takes longer for the recording device to be switched on than the length of some animal calls there could be a systematic underestimation of density.

Accuracy and Precision. Based on our simulations we believe that the gREM has the potential to produce accurate estimates for many different species, using either camera traps or acoustic detectors. However the precision of the gREM differed between submodels. For example, when the sensor and signal width were smaller than the precision of the model was reduced, so when choosing a sensor for use in a gREM study the detection width should be maximised, and if the study species has a narrow signal directionality other aspects of the study protocol, such as length of the survey, should be used to compensate.

The precision of the gREM is greatly affected by the number of captures that are collected, the coefficient of variation falls dramatically between 10 and 60 captures and then after this continues to slowly reduce. At 100 captures the submodels reach 10% coefficient of variation, considered to a very good level of precision

(Thomas & Marques, 2012). Many current studies do not reach this level of precision, with most studies reporting coefficient of variations greater than the 10% level (O'Brien *et al.*, 2003; Proctor *et al.*, 2010; Foster & Harmsen, 2012). The length of surveys in the field will need to be adjusted so that enough data can be collected to reach this level of precision. Populations of fast moving animals or populations with large densities will require less survey effort than those with slow moving or low densities.

The gREM was both accurate and precise for all the movement models we tested (stop-start movement and correlated random walks). However these movement models are still simple representations of true animal movement which are dependent on multiple factors such as behavioural state and existence of home ranges (Smouse *et al.*, 2010). The accuracy of the gREM may be affected by the interaction between the movement model and the size of the detection radius. We have studied a relatively long step length compared to the size of the detection radius, and therefore the chance of catching the same animal multiple times within a short space of time was reduced and there is little affect on the precision of the model (Figure 8b). However if the ratio of step length to detection radius was smaller then this may decrease the precision of the model, however this should not decrease its accuracy.

Although we have used simulations to validate the gREM submodels, much more robust testing is needed. Although difficult, proper field test validation would be required before the models could be fully trusted. The REM (Rowcliffe *et al.*, 2008) has already been field tested, and both Rowcliffe *et al.* (2008) and Zero *et al.* (2013) both found that the REM was an effective manner of estimating animal densities (Rowcliffe *et al.*, 2008; Zero *et al.*, 2013). In some taxa gold standard methods of estimating animal density exist, such as capture mark recapture (Sollmann *et al.*, 2013). Where these gold standard exist or true numbers are known, a simultaneous gREM study could be completed to test the accuracy under field conditions, similar to the tests that Rowcliffe *et al.* (2008) completed with the REM. An easier way to continue to evaluate the models is to run more extensive simulations which break the assumptions of the analytical models. The main element that

cannot be analytically treated is the complex movement of real animals. Therefore testing these methods against true animal traces, or more complex movement models would be required.

Within the simulation we have assumed an equal density across the entire world, however in a field environment the situation would be much more complex, with additional variation coming from local changes in density between camera sites. We allowed the sensor to be stationary and on all the time, negating the triggering, and time expansion issues that could exist in real life. In the simulation we ran the speed of the animal as 40 km day⁻¹, the largest day range of terrestrial animals (Carbone *et al.*, 2005). Other speed values should not alter the accuracy of the gREM (precision would be affected, all else being equal, since slower speeds produce fewer records). We also assume perfect knowledge of the average speed of an animal and size of the detection zone, and instant triggering of the camera. All of which may lead to possible bias or a decrease in precision.

Implications for conservation. The gREM is available for the estimation of density of a number of taxa where no, or few, accurate methods currently exist to measure absolute animal density (Thomas & Marques, 2012). The species that can now be studied may be of importance to conservation, for example current methods of density estimation for the threatened Franciscana dolphin may result in underestimation of numbers (Crespo *et al.*, 2010). This new method may be important for the study of zoonotic diseases, for example estimating population sizes of bats, which are important reservoir of infectious disease that affect humans, livestock and wildlife (Calisher *et al.*, 2006). In addition, the gREM will make it possible to measure the density of animals which may be useful in quantifying ecosystem services, such as studying the levels of songbirds which are known to have a positive influence on pest control in coffee production (Jirinec *et al.*, 2011). The gREM is suitable for any species that would be consistently recorded within range of a detector, such as bats (Kunz *et al.*, 2009), songbirds (Buckland & Handel, 2006), whales (Marques *et al.*, 2009) or forest primates (Hassel-Finnegan *et al.*, 2008). With increasing technological capabilities, this list of species is likely to increase dramatically.

Importantly the camera trapping and acoustic recording that the gREM use are noninvasive and do not require individual marking (Jewell, 2013) or naturally identifying marks (as required for mark-recapture models). This makes them suitable for large, continuous monitoring projects with limited human resources (Kelly *et al.*, 2012). It also makes them suitable for species that are under pressure, species that cannot naturally be individually recognised or species that are difficult or dangerous to catch (Thomas & Marques, 2012).

1. ACKNOWLEDGMENTS

REFERENCES

- Acevedo, M.A. & Villanueva-Rivera, L.J. (2006) Using automated digital recording systems as effective tools for the monitoring of birds and amphibians. *Wildlife Society Bulletin*, **34**, 211–214.
- Adams, R.A., Pedersen, S.C., Walters, C., Collen, A., Lucas, T., Mroz, K., Sayer, C. & Jones, K. (2013) *Challenges of Using Bioacoustics to Globally Monitor Bats*, pp. 479–499. Springer New York.
- Ahlen, I. & Baagøe, H.J. (1999) Use of ultrasound detectors for bat studies in europe: experiences from field identification, surveys, and monitoring. *Acta Chiropterologica*, **1**, 137–150.
- Anderson, D.R. (2001) The need to get the basics right in wildlife field studies. *Wildlife Society Bulletin*, **29**, 1294–1297.
- Barlow, J. & Taylor, B. (2005) Estimates of sperm whale abundance in the north-eastern temperate pacific from a combined acoustic and visual survey. *Marine Mammal Science*, **21**, 429–445.
- Blumstein, D.T., Mennill, D.J., Clemins, P., Girod, L., Yao, K., Patricelli, G., Deppe, J.L., Krakauer, A.H., Clark, C., Cortopassi, K.A. *et al.* (2011) Acoustic monitoring in terrestrial environments using microphone arrays: applications, technological considerations and prospectus. *Journal of Applied Ecology*, **48**, 758–767.
- Borchers, D., Distiller, G., Foster, R., Harmsen, B. & Milazzo, L. (2014) Continuous-time spatially explicit capture–recapture models, with an application to a jaguar camera-trap survey. *Methods in Ecology and Evolution*.

- 456 Brusa, A. & Bunker, D.E. (2014) Increasing the precision of canopy closure es-
457 timates from hemispherical photography: Blue channel analysis and under-
458 exposure. *Agricultural and Forest Meteorology*, **195**, 102–107.
- 459 Buckland, S.T. & Handel, C. (2006) Point-transect surveys for songbirds: robust
460 methodologies. *The Auk*, **123**, 345–357.
- 461 Buckland, S.T., Marsden, S.J. & Green, R.E. (2008) Estimating bird abundance:
462 making methods work. *Bird Conservation International*, **18**, S91–S108.
- 463 Calisher, C., Childs, J., Field, H., Holmes, K. & Schountz, T. (2006) Bats: important
464 reservoir hosts of emerging viruses. *Clinical Microbiology Reviews*, **19**, 531–545.
- 465 Carbone, C., Cowlishaw, G., Isaac, N.J. & Rowcliffe, J.M. (2005) How far do ani-
466 mals go? Determinants of day range in mammals. *The American Naturalist*, **165**,
467 290–297.
- 468 Clark, C.W. (1995) Application of US Navy underwater hydrophone arrays for
469 scientific research on whales. *Reports of the International Whaling Commission*, **45**,
470 210–212.
- 471 Clement, M.J. & Castleberry, S.B. (2013) Estimating density of a forest-dwelling
472 bat: a predictive model for rafinesque’s big-eared bat. *Population Ecology*, **55**,
473 205–215.
- 474 Crespo, E.A., Pedraza, S.N., Grandi, M.F., Dans, S.L. & Garaffo, G.V. (2010) Abun-
475 dance and distribution of endangered franciscana dolphins in argentine waters
476 and conservation implications. *Marine Mammal Science*, **26**, 17–35.
- 477 Cutler, T.L. & Swann, D.E. (1999) Using remote photography in wildlife ecology:
478 a review. *Wildlife Society Bulletin*, **27**, 571–581.
- 479 Damuth, J. (1981) Population density and body size in mammals. *Nature*, **290**,
480 699–700.
- 481 Depraetere, M., Pavoine, S., Jiguet, F., Gasc, A., Duvail, S. & Sueur, J. (2012) Mon-
482 itoring animal diversity using acoustic indices: implementation in a temperate
483 woodland. *Ecological Indicators*, **13**, 46–54.
- 484 Elphick, C.S. (2008) How you count counts: the importance of methods research
485 in applied ecology. *Journal of Applied Ecology*, **45**, 1313–1320.
- 486 Everatt, K.T., Andresen, L. & Somers, M.J. (2014) Trophic scaling and occupancy
487 analysis reveals a lion population limited by top-down anthropogenic pressure

- in the limpopo national park, mozambique. *PloS one*, **9**, e99389.
- Foster, R.J. & Harmsen, B.J. (2012) A critique of density estimation from camera-trap data. *The Journal of Wildlife Management*, **76**, 224–236.
- Harris, D., Matias, L., Thomas, L., Harwood, J. & Geissler, W.H. (2013) Applying distance sampling to fin whale calls recorded by single seismic instruments in the northeast atlantic. *The Journal of the Acoustical Society of America*, **134**, 3522–3535.
- Hassel-Finnegan, H.M., Borries, C., Larney, E., Umponjan, M. & Koenig, A. (2008) How reliable are density estimates for diurnal primates? *International Journal of Primatology*, **29**, 1175–1187.
- Hayes, J.P. (2000) Assumptions and practical considerations in the design and interpretation of echolocation-monitoring studies. *Acta Chiropterologica*, **2**, 225–236.
- Hutchinson, J.M.C. & Waser, P.M. (2007) Use, misuse and extensions of “ideal gas” models of animal encounter. *Biological Reviews of the Cambridge Philosophical Society*, **82**, 335–359.
- Jewell, Z. (2013) Effect of monitoring technique on quality of conservation science. *Conservation Biology*, **27**, 501–508.
- Jirinec, V., Campos, B.R. & Johnson, M.D. (2011) Roosting behaviour of a migratory songbird on jamaican coffee farms: landscape composition may affect delivery of an ecosystem service. *Bird Conservation International*, **21**, 353–361.
- Jones, K.E., Bielby, J., Cardillo, M., Fritz, S.A., O'Dell, J., Orme, C.D.L., Safi, K., Sechrest, W., Boakes, E.H., Carbone, C., Connolly, C., Cutts, M.J., Foster, J.K., Grenyer, R., Habib, M., Plaster, C.A., Price, S.A., Rigby, E.A., Rist, J., Teacher, A., Bininda-Emonds, O.R.P., Gittleman, J.L., Mace, G.M., Purvis, A. & Michener, W.K. (2009) Pantheria: a species-level database of life history, ecology, and geography of extant and recently extinct mammals. *Ecology*, **90**, 2648.
- Jones, K.E., Russ, J.A., Bashta, A.T., Bilhari, Z., Catto, C., Csősz, I., Gorbachev, A., Győrfi, P., Hughes, A., Ivashkiv, I., Koryagina, N., Kurali, A., Langton, S., Collen, A., Margiean, G., Pandourski, I., Parsons, S., Prokofev, I., Szodoray-Paradi, A., Szodoray-Paradi, F., Tilova, E., Walters, C.L., Weatherill, A. &

- 519 Zavarzin, O. (2013) *Indicator Bats Program: A System for the Global Acoustic Moni-*
520 *toring of Bats*, pp. 211–247. Wiley-Blackwell.
- 521 Karanth, K. (1995) Estimating tiger (*Panthera tigris*) populations from camera-trap
522 data using capture–recapture models. *Biological Conservation*, **71**, 333–338.
- 523 Kelly, M.J., Betsch, J., Wultsch, C., Mesa, B. & Mills, L.S. (2012) Noninvasive sam-
524 pling for carnivores. *Carnivore ecology and conservation: a handbook of techniques*
525 (*L Boitani and RA Powell, eds*) Oxford University Press, New York, pp. 47–69.
- 526 Kessel, S., Cooke, S., Heupel, M., Hussey, N., Simpfendorfer, C., Vagle, S. & Fisk, A.
527 (2014) A review of detection range testing in aquatic passive acoustic telemetry
528 studies. *Reviews in Fish Biology and Fisheries*, **24**, 199–218.
- 529 Kimura, S., Akamatsu, T., Dong, L., Wang, K., Wang, D., Shibata, Y. & Arai, N.
530 (2014) Acoustic capture-recapture method for towed acoustic surveys of echolo-
531 cating porpoises. *The Journal of the Acoustical Society of America*, **135**, 3364–3370.
- 532 Kunz, T.H., Betke, M., Hristov, N.I. & Vonhof, M. (2009) Methods for assessing
533 colony size, population size, and relative abundance of bats. *Ecological and be-*
534 *havioral methods for the study of bats* (*TH Kunz and S Parsons, eds*) 2nd ed Johns
535 *Hopkins University Press, Baltimore, Maryland*, pp. 133–157.
- 536 Lammers, M.O. & Au, W.W. (2003) Directionality in the whistles of hawaiian spin-
537 ner dolphins (*stenella longirostris*): A signal feature to cue direction of move-
538 ment? *Marine Mammal Science*, **19**, 249–264.
- 539 Lewis, T., Gillespie, D., Lacey, C., Matthews, J., Danbolt, M., Leaper, R.,
540 McLanaghan, R. & Moscrop, A. (2007) Sperm whale abundance estimates from
541 acoustic surveys of the ionian sea and straits of sicily in 2003. *Journal of the Ma-*
542 *rine Biological Association of the United Kingdom*, **87**, 353–357.
- 543 Manzo, E., Bartolommei, P., Rowcliffe, J.M. & Cozzolino, R. (2012) Estimation of
544 population density of european pine marten in central italy using camera trap-
545 ping. *Acta Theriologica*, **57**, 165–172.
- 546 Marcoux, M., Auger-Méthé, M., Chmelnitsky, E.G., Ferguson, S.H. & Humphries,
547 M.M. (2011) Local passive acoustic monitoring of narwhal presence in the cana-
548 dian arctic: a pilot project. *Arctic*, **64**, 307–316.
- 549 Marques, T.A., Munger, L., Thomas, L., Wiggins, S. & Hildebrand, J.A. (2011) Es-
550 timating North Pacific right whale (*Eubalaena japonica*) density using passive

- acoustic cue counting. *Endangered Species Research*, **13**, 163–172.
- Marques, T.A., Thomas, L., Ward, J., DiMarzio, N. & Tyack, P.L. (2009) Estimating cetacean population density using fixed passive acoustic sensors: An example with Blainville’s beaked whales. *The Journal of the Acoustical Society of America*, **125**, 1982–1994.
- O’Brien, T.G., Kinnaird, M.F. & Wibisono, H.T. (2003) Crouching tigers, hidden prey: Sumatran tiger and prey populations in a tropical forest landscape. *Animal Conservation*, **6**, 131–139.
- O’Farrell, M.J. & Gannon, W.L. (1999) A comparison of acoustic versus capture techniques for the inventory of bats. *Journal of Mammalogy*, **80**, 24–30.
- Proctor, M., McLellan, B., Boulanger, J., Apps, C., Stenhouse, G., Paetkau, D. & Mowat, G. (2010) Ecological investigations of grizzly bears in Canada using DNA from hair, 1995–2005: a review of methods and progress. *Ursus*, **21**, 169–188.
- Purvis, A., Gittleman, J.L., Cowlishaw, G. & Mace, G.M. (2000) Predicting extinction risk in declining species. *Proceedings of the Royal Society of London Series B: Biological Sciences*, **267**, 1947–1952.
- Richter-Dyn, N. & Goel, N.S. (1972) On the extinction of a colonizing species. *Theoretical Population Biology*, **3**, 406–433.
- Rogers, T.L., Ciaglia, M.B., Klinck, H. & Southwell, C. (2013) Density can be misleading for low-density species: benefits of passive acoustic monitoring. *Public Library of Science One*, **8**, e52542.
- Rovero, F., Zimmermann, F., Berzi, D. & Meek, P. (2013) “which camera trap type and how many do I need?” a review of camera features and study designs for a range of wildlife research applications. *Hystrix*, **24**, 148–156.
- Rowcliffe, J.M. & Carbone, C. (2008) Surveys using camera traps: are we looking to a brighter future? *Animal Conservation*, **11**, 185–186.
- Rowcliffe, J., Field, J., Turvey, S. & Carbone, C. (2008) Estimating animal density using camera traps without the need for individual recognition. *Journal of Applied Ecology*, **45**, 1228–1236.
- Schmidt, B.R. (2003) Count data, detection probabilities, and the demography, dynamics, distribution, and decline of amphibians. *Comptes Rendus Biologies*, **326**, 119–124.

- 583 Smouse, P.E., Focardi, S., Moorcroft, P.R., Kie, J.G., Forester, J.D. & Morales, J.M.
 584 (2010) Stochastic modelling of animal movement. *Philosophical Transactions of the*
 585 *Royal Society B: Biological Sciences*, **365**, 2201–2211.
- 586 Soisalo, M.K. & Cavalcanti, S. (2006) Estimating the density of a jaguar population
 587 in the Brazilian Pantanal using camera-traps and capture-recapture sampling in
 588 combination with GPS radio-telemetry. *Biological Conservation*, **129**, 487–496.
- 589 Sollmann, R., Gardner, B., Chandler, R.B., Shindle, D.B., Onorato, D.P., Royle, J.A.
 590 & O’Connell, A.F. (2013) Using multiple data sources provides density estimates
 591 for endangered florida panther. *Journal of Applied Ecology*, **50**, 961–968.
- 592 SymPy Development Team (2014) *SymPy: Python library for symbolic mathematics*.
 593 Team, R.C. (2014) *R: A Language and Environment for Statistical Computing*. R Foun-
 594 dation for Statistical Computing, Vienna, Austria.
- 595 Thomas, L. & Marques, T.A. (2012) Passive acoustic monitoring for estimating an-
 596 imal density. *Acoustics Today*, **8**, 35–44.
- 597 Trolle, M. & Kéry, M. (2003) Estimation of ocelot density in the Pantanal using
 598 capture-recapture analysis of camera-trapping data. *Journal of Mammalogy*, **84**,
 599 607–614.
- 600 Trolle, M., Noss, A.J., Lima, E.D.S. & Dalponte, J.C. (2007) Camera-trap studies of
 601 maned wolf density in the Cerrado and the Pantanal of Brazil. *Biodiversity and*
 602 *Conservation*, **16**, 1197–1204.
- 603 Wright, S.J. & Hubbell, S.P. (1983) Stochastic extinction and reserve size: a focal
 604 species approach. *Oikos*, pp. 466–476.
- 605 Yapp, W. (1956) The theory of line transects. *Bird Study*, **3**, 93–104.
- 606 Zero, V.H., Sundaresan, S.R., O’Brien, T.G. & Kinnaird, M.F. (2013) Monitoring
 607 an endangered savannah ungulate, Grevy’s zebra (*Equus grevyi*): choosing a
 608 method for estimating population densities. *Oryx*, **47**, 410–419.

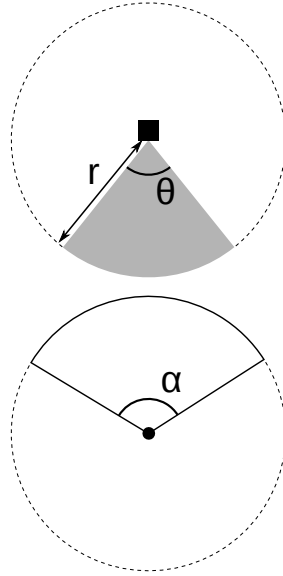


FIGURE 1. Representation of sensor detection width and animal signal width. The filled square and circle represent a sensor and an animal, respectively; θ , sensor detection width (radians); r , sensor detection distance; dark grey shaded area, sensor detection zone; α , animal signal width (radians). Dashed lines around the filled square and circle represents the maximum extent of θ and α , respectively.

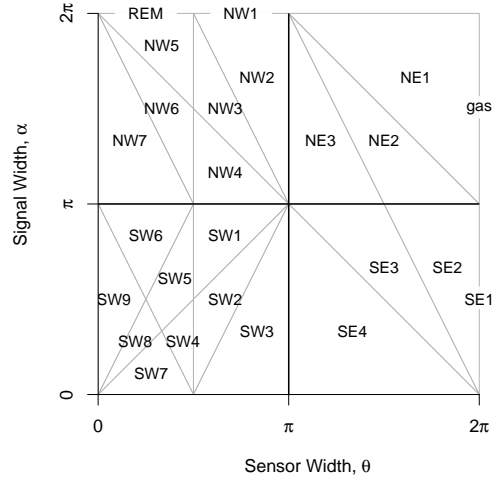


FIGURE 2. Locations where derivation of the average profile \bar{p} is the same for different combinations of sensor detection width and animal signal width. Symbols within each polygon refer to each gREM submodel named after their compass point, except for Gas and REM which highlight the position of these previously derived models within the gREM. Symbols on the edge of the plot are for submodels with $\alpha, \theta = 2\pi$

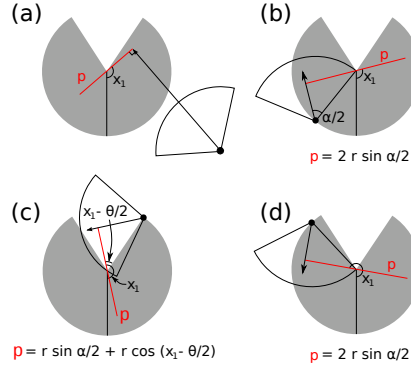


FIGURE 3. An overview of the derivation of SE2. The filled circles represent animals, with the animal signal shown as an unfilled sector and the direction of movement shown as an arrow. The detection zone of the sensor is shown as filled grey sectors with a detection distance of r . The vertical black line within the circle shows the direction the sensor is facing; θ , sensor detection width; α , animal signal width. The profile p (the line an animal must pass through in order to be captured) is shown in red and x_1 is the focal angle, where (a) shows the location of x_1 . The derivation of p changes as the animal approaches the sensor from different directions where (b) is the derivation of p when x_1 is in the interval $[\frac{\pi}{2}, \frac{\pi}{2} + \frac{\theta}{2} - \frac{\alpha}{2}]$, (c) p when x_1 is in the interval $[\frac{\pi}{2} + \frac{\theta}{2} - \frac{\alpha}{2}, \frac{5\pi}{2} - \frac{\theta}{2} - \frac{\alpha}{2}]$ and (d) p when x_1 is in the interval $[\frac{5\pi}{2} - \frac{\theta}{2} - \frac{\alpha}{2}, \frac{3\pi}{2}]$. The resultant equation for p is shown beneath each figure.

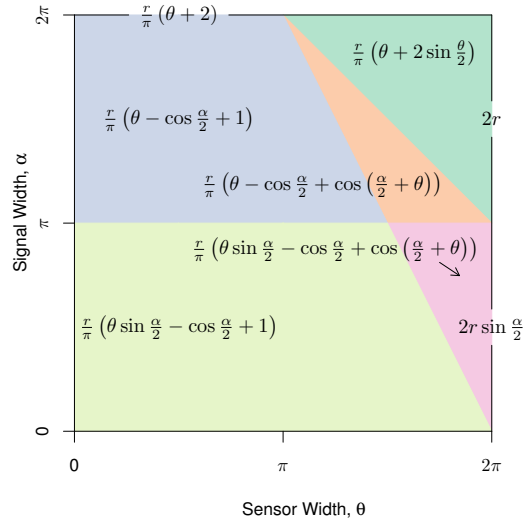


FIGURE 4. Expressions for the average profile width, \bar{p} , given sensor and signal widths. Despite independent derivation within each block, many models result in the same expression. These are collected together and presented as one block of colour. Expressions on the edge of the plot are for submodels with $\alpha, \theta = 2\pi$.

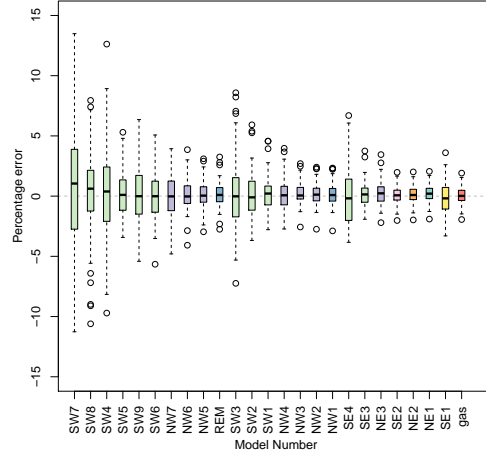


FIGURE 5. Simulation model results of the accuracy and precision for gREM submodels. The percentage error between estimated and true density for each gREM submodel is shown within each box plot, where the black line represents the median percentage error across all simulations, boxes represent the the middle 50% of the data, whiskers represent variability outside the upper and lower quartiles with outliers plotted as individual points. Box colours correspond to the expressions for average profile width \bar{p} given in Figure 4.

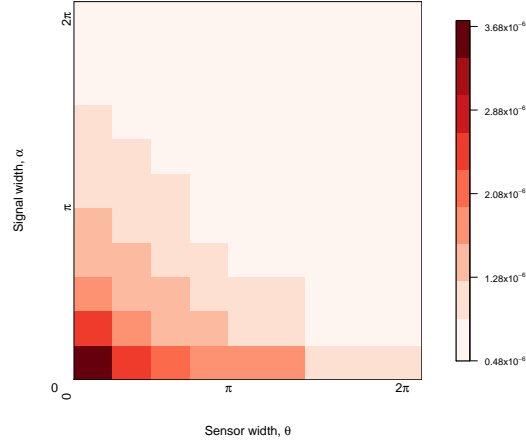


FIGURE 6. Simulation model results of the gREM precision given a range of sensor and signal widths, shown by the standard deviation of the error between the estimated and true densities. Standard deviations are shown from deep red to pink, representing high to low values between 0.483×10^{-6} to 3.74×10^{-6} .

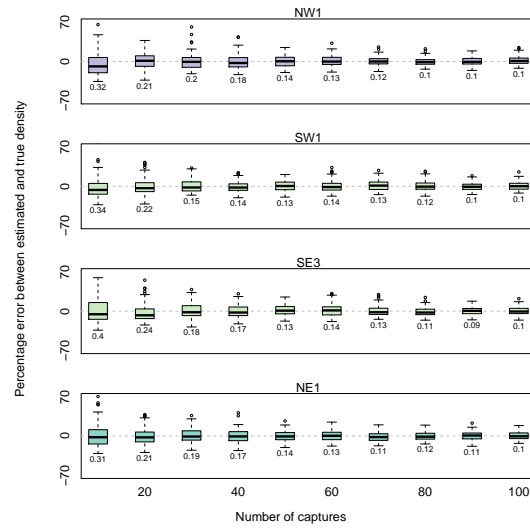


FIGURE 7. Simulation model results of the accuracy and precision of four gREM submodels (NW1, SW1, SE3 and NE1) given different numbers of captures. The percentage error between estimated and true density within each gREM sub model for capture rate is shown within each box plot. Sensor and signal widths vary between submodels. The number beneath each plot represents the coefficient of variation. The colour of each box plot corresponds to the expressions for average profile width \bar{p} given in Figure 4.

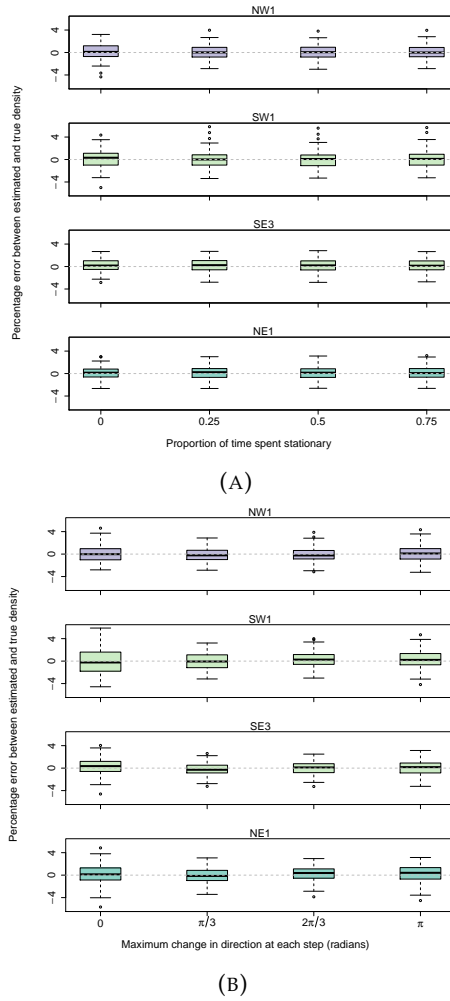


FIGURE 8. Simulation model results of the accuracy and precision of four gREM submodels (NW1, SW1, SE3 and NE1) given different movement models where (A) amount of time spent stationary (stop-start movement) and (B) maximum change in direction at each step (correlated random walk model). The percentage error between estimated and true density within each gREM sub model for the different movement models is shown within each box plot. The simple model is represented where time and maximum change in direction equals 0. The colour of each box plot corresponds to the expressions for average profile width \bar{p} given in Figure 4.